Revista Mexicana de Física
ISSN: 0035-001X
rmf@ciencias.unam.mx
Sociedad Mexicana de Física A.C.
México

Castrejón-García, R.; Castrejón-Pita, J.R.; Martin, G.D.; Hutchings, I.M.
The shadowgraph imaging technique and its modern application to fluid jets and drops
Revista Mexicana de Física, vol. 57, núm. 3, junio, 2011, pp. 266-275
Sociedad Mexicana de Física A.C.
Distrito Federal, México

The shadowgraph imaging technique and its modern application to fluid jets and drops

R. Castrejón-García[a], J.R. Castrejón-Pita[b], G.D. Martin[b], and I.M. Hutchings[b]
[a]*Centro de Investigación en Energía, Universidad Nacional Autónoma de México, Priv. Xochicalco s/n, Temixco, Mor. 62580, México.*
[b]*Institute for Manufacturing, University of Cambridge, 17 Charles Babbage Road, Cambridge, CB3 0FS, United Kingdom.*

Recibido el 7 de febrero de 2011; aceptado el 11 de abril de 2011

The shadowgraph technique is discussed in terms of some modern application to fluid visualization and the characterization of free-surface flows. A brief description of shadowgraph photography is presented which emphasizes the parameters which need to be controlled to obtain useful images for digital processing and analysis. Several examples of shadowgraph images are presented together with their analysis to exemplify the variety of quantitative measurements that are possible with modern imaging tools. Three experimental setups were developed for different novel applications at different length scales: centimeter-long jets, millimeter-size sprays and micrometer-size droplets. The components used for these shadowgraph imaging systems range from standard photographic flash sources to specialized spark flash lamps and from single lens reflex (SLR) camera lenses to purpose-built systems with research-grade optical elements. Image analysis was developed and used to derive various types of information from the different systems. For jets it was used to determine the dynamic surface tension of the jetted fluid, for sprays it was employed to determine the ligament-droplet size distribution along the jetting axis and in inkjet printing it was used to determine the angular deviation and terminal speed of the jets and droplets.

Keywords: Sprays; droplets; jets; shadowgraph.

La técnica de fotografía de sombra se discute en términos de algunas de sus aplicaciones modernas en la visualización de fluidos y la caracterización de flujos con superficie libre. La fotografía de sombra se describe brevemente, haciendo hincapié en los parámetros que se deben controlar para obtener imágenes aptas para el procesamiento digital y análisis. Se presentan también algunos ejemplos de imágenes de fotografía de sombra con su correspondiente análisis, para ejemplificar la variedad de mediciones cuantitativas que pueden hacerse con las herramientas modernas de imagen. Se desarrollaron tres montajes experimentales para algunas aplicaciones novedosas: chorros de centímetros de largo, aerosoles de milímetros de tamaño y gotas de micras de tamaño. Los componentes que se utilizan en estos sistemas de fotografía de sombra van desde fuentes de destello estándar, hasta lámparas especializadas de destello con chispa; y desde cámaras réflex de un solo lente (SLR), hasta sistemas construidos expresamente con elementos ópticos de alta calidad. El método de análisis de las imágenes fue desarrollado para obtener diversos tipos de información de los diferentes sistemas; en los chorros se usa para encontrar la tensión superficial dinámica del fluido eyectado; en los aerosoles se usa para determinar la distribución de tamaño de los ligamentos y las gotas a lo largo del eje del aerosol; y en los chorros de impresión de tinta se usa para determinar su desviación angular y la velocidad terminal de los chorros y las gotas.

Descriptores: Aerosoles; gotas; chorros; fotografía de sombra.

PACS: 47.80.Jk; 47.55.db; 47.80.Jk; 81.15.Rs; 82.70.Rr

1. Introduction

Among the different optical techniques used in the study of particles, liquids or gases in motion, shadowgraph imaging stands out as a usually inexpensive but powerful technique. Traditionally, the shadowgraph technique has been often used to qualitatively study the dynamics of fluids through the visualization of flows or the recording of flow streamlines. The aim of this paper is to provide some examples where shadowgraphy can be used in conjunction with digital image processes to quantitatively determine fluid and flow properties, and to show how shadowgraphy can be used as a quantitative technique.

In general terms, shadowgraph photography highlights the difference in refractive index at the interface between a body and its surroundings (medium), or between media, [1]. With back-illumination, the light that does not interact with the object produces a bright background, whereas the light refracted at the interface is dispersed and thus the interface appears dark. As a consequence, shadowgraph images consist of a bright background and the shadows of the interfaces between regions with different refractive indexes. Generally speaking, the use of shadowgraphy is appropriate when the medium being studied is transparent and for media with large differences in refractive index (*e.g.* air and water). Most shadowgraph systems consist of two main components: the illumination source and the recording element. In brief, the

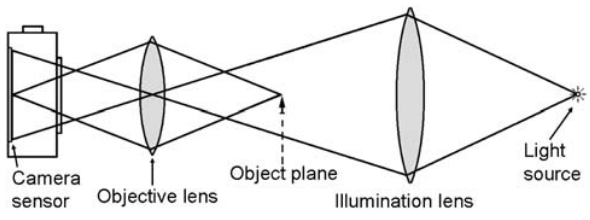

FIGURE 1. Generic diagram of a shadowgraph system.

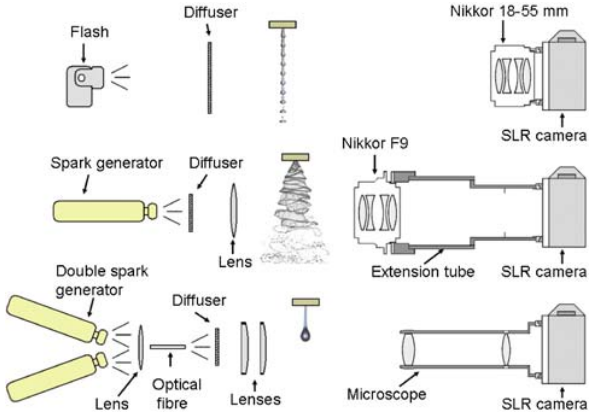

FIGURE 2. (Colour online) Schematic diagrams of the optical and illumination setups used for the different applications. The top illustration shows the system used for jets, the middle one for sprays and the bottom for droplets. All the Nikon DSLR cameras had a 23.6×15.8 mm 10.4 Megapixel CCD sensor. Dimensions not to scale.

aim of the illumination arrangement is to obtain a homogeneous background at the recording sensor and to provide the light which is refracted by the object or media under study. The recording system contains the optical elements required to form and record an image of the object's silhouette or shadow. Usually, short-duration illumination is provided by a flash-lamp, spark generator or LED, and film or a CCD sensor are used as recording elements.

Although the optical principles behind this technique are simple, it does not always lend itself to easy laboratory implementation. Figure 1 shows a typical schematic view of a shadowgraph system and exemplifies the simplicity of the design. However, there are several variables that must be controlled and adjusted to obtain useful images for analysis. Generically, all shadowgraph systems are similar although they differ in their detailed components. The specifications of these components are important as the contrast, sharpness and brightness of shadowgraph images depend on parameters such as the magnification, light sensitivity, field of view, depth of field and focal length of the optical system. Ideally, a shadowgraph system should be designed to fulfil some designated conditions of field of view, sharpness and brightness but in practice, some systems are designed more pragmatically, based on the (local or commercial) availability of optical components. Primarily, the size of the feature to be identified on the images determines the optical magnification which is the dominant specification of the optical components. Other variables such as the depth of field and the sensor size and sensitivity are often chosen and adjusted to improve the quality of the image formed on the sensor. Additional variables such as the optical distortion and the working distance are usually chosen based on component availability but with the aim to enhance the image quality or to facilitate the operation of the system. To visualize centimeter or millimeter-scale objects, conventional photography offers a wide variety of optical elements such as lenses, flash light sources and shutters. However, for micrometer-scale experiments, the ability to choose the depth of field and the working distance independently is restricted by the availability of microscope objectives and optical zoom assemblies. These restrictions may cause difficulties in the use of shadowgraphy for a particular application and need to be known and controlled as part of the design of the system.

Shadowgraph photography has advantages over other visualization techniques because it is non-invasive and allows the recording and in many cases measurement of several characteristics such as interface speed and direction of motion, and object sizes [2,3]. In this paper, it is shown how the processing of shadowgraph images can be used to quantitatively determine important properties of jets, sprays and droplets. It is also shown that this visualization technique combined with digital image analysis can be employed to investigate and quantitatively determine: i) the dynamic surface tension and the the surface profile of modulated jets in the Rayleigh regime, ii) the ligament and droplet size distribution of sprays, iii) the straightness or angle of deviation of jetted droplets and iv) the effects of nozzle defects on the directionality of jetted droplets. The image analysis method used in these studies is simple and generic and can be reproduced in several numerical computing environments and programming languages (*e.g.* Matlab, LabView, or Visual C). These analyzes are based on tracing the outlines of objects in shadowgraph images through the detection of local colour or intensity level gradients. Once the feature boundaries are found and recorded, this information is then used to measure the sizes of the objects and their positions. This data is then utilized to measure different properties according to the particular application.

2. Shadowgraph imaging

The three imaging systems described below were conceived and built to cover three different regimes found in the ejection of liquids through nozzles: single droplets, jets and sprays. These regimes are ultimately determined by the properties of the fluid, the geometry of the nozzle and the pressure history applied to the liquid. Generally, a single short pressure pulse produces a single droplet, a sustained high pressure produces a jet and a long pressure pulse of higher amplitude creates an spray [5,10]. These three modes of fluid ejection are important as they are extensively used in industry to deliver and deposit fluids in a variety of applications. In addition, the physical dimensions of the experimental setups were chosen to demonstrate the use of the shadowgraph technique and digital image analysis over a wide range of conditions, ranging from centimeter-long jets down to micrometer-sized droplets. As a consequence, most of the optical elements were different between these three systems. The only component common to all systems was the 23.6×15.8 mm 10 Megapixel CCD camera sensor (in Nikon D40x and D80 DSLR cameras) which was used to capture all the shadowgraph images in this work. Fig. 2 illustrates the various components used.

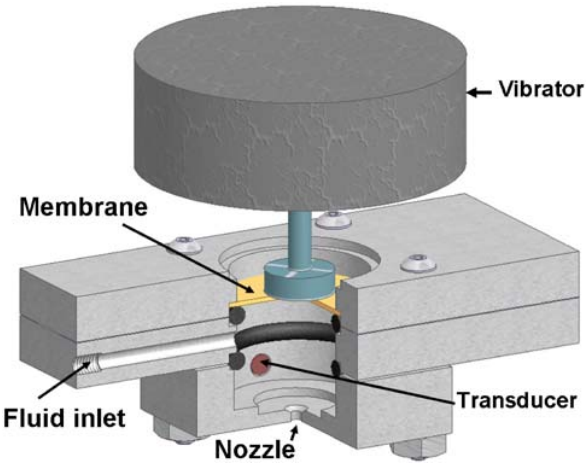

FIGURE 3. (Colour online) Sectional view of the millimeter-scale printhead. Relative sizes are in correct proportion. The nozzle shape consists of a 45 degree (half-angle) conical inlet, followed by a parallel cylindrical section 2.2 mm in diameter and 2.2 mm long.

2.1. Jets

The first setup was a shadowgraph system built to observe and record instantaneous images of a harmonically disturbed continuous liquid jet. The interest in these observations lies in the fact that the dynamics of such a system were theoretically described by Rayleigh (for inviscid liquids) in 1878 and by Weber (for viscous fluids) in 1931, [11,12] and [2]. The Rayleigh and Weber models predict the surface profile of a weakly modulated liquid jet emerging from a cylindrical nozzle. These models can be used in conjunction with shadowgraph imaging and analysis of centimeter-long jets to estimate the dynamic surface tension of the jetted fluid and determine the speed and size of the droplets formed after jet break-up. These studies are relevant to the printing industry as modulated jets form the basis of continuous ink-jet printers.

The model printhead used to generate and harmonically disturb the jets is a modified version of a design described elsewhere [10]. Briefly, it consists of a sealed, pressurized liquid-filled chamber with the outlet nozzle in its lower surface and a rubber membrane forming the upper face, as shown schematically in Fig. 3. The membrane is in contact with the liquid on one surface and with an electromagnetic vibrator on the other, and is used to transmit the oscillatory motion from the actuator to the fluid. The vibrator (LDS Test and Measurement Ltd, model V201) is driven by an amplifier (Nikkai 250, total harmonic distortion $<0.025\%$) connected to a function generator (TTi model TG550). The liquid is fed into the chamber by a regulated pump (Promotec model BL58) and emerges from the nozzle as a jet. The jet velocity is adjusted by varying the power applied to the pump and the pressure in the chamber is measured with a dynamic pressure transducer (Entran Sensors & Electronics, EPX-N12-1B) in

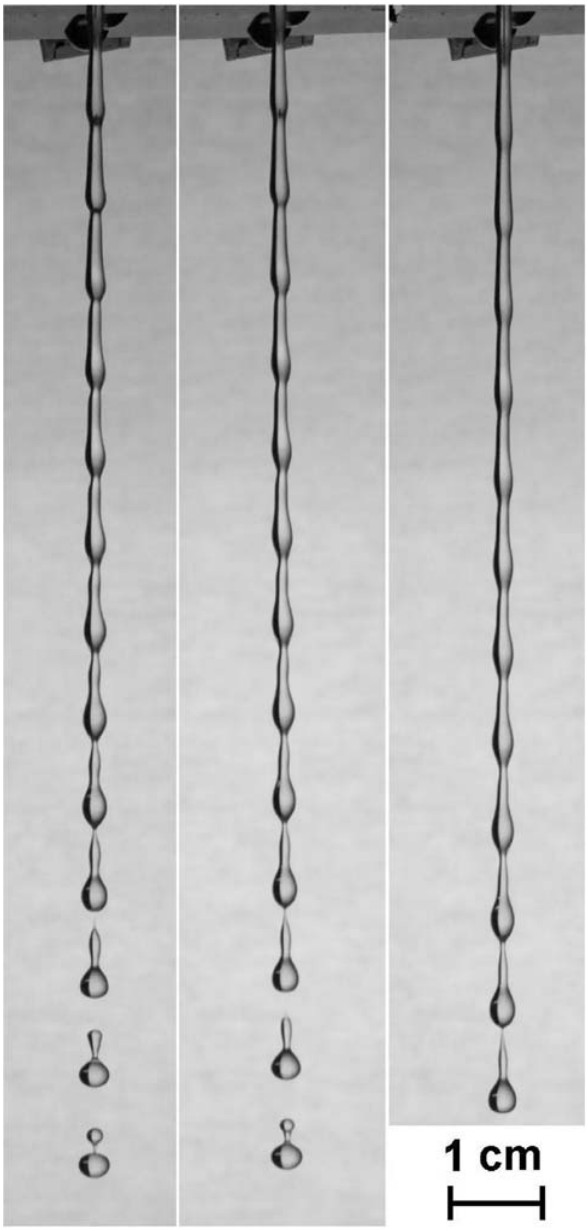

FIGURE 4. Examples of shadowgraph pictures of jets formed from glycerol/water mixtures. The jet is modulated with a 333 Hz sinusoidal waveform and breaks up into droplets with a speed of 3.9 m/s. Pressure modulation amplitudes are 4.8%, 3.5% and 2.6% respectively.

contact with the liquid. This transducer is used to monitor the amplitude and shape of the pressure waveform produced by the function generator. In these experiments, a solution of 74.7% (by mass) pure glycerol in triple-distilled water was jetted through a 2.2 mm diameter nozzle with a 45 degree (included angle) conical inlet and a cylindrical section 2.2 mm long. The static pressure used to jet the fluid at 3.50 ± 0.03 m/s was 11.4 kPa. The vibrator was set up to produce a pressure modulation amplitude of 1% of that value

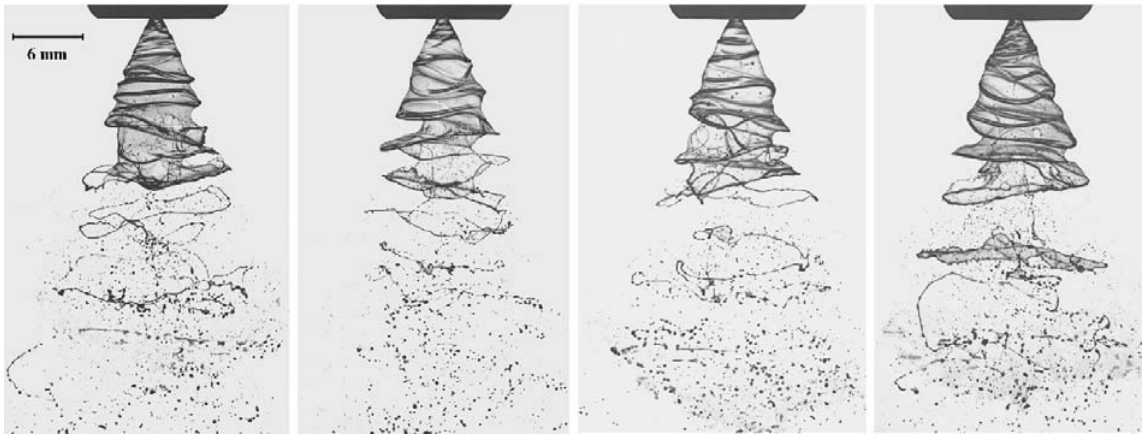

FIGURE 5. (Colour online) Shadowgraph images of quenching oil at 38°C emerging from a 1.2 mm atomizer nozzle. The average terminal speed of the spray droplets is 15 m/s.

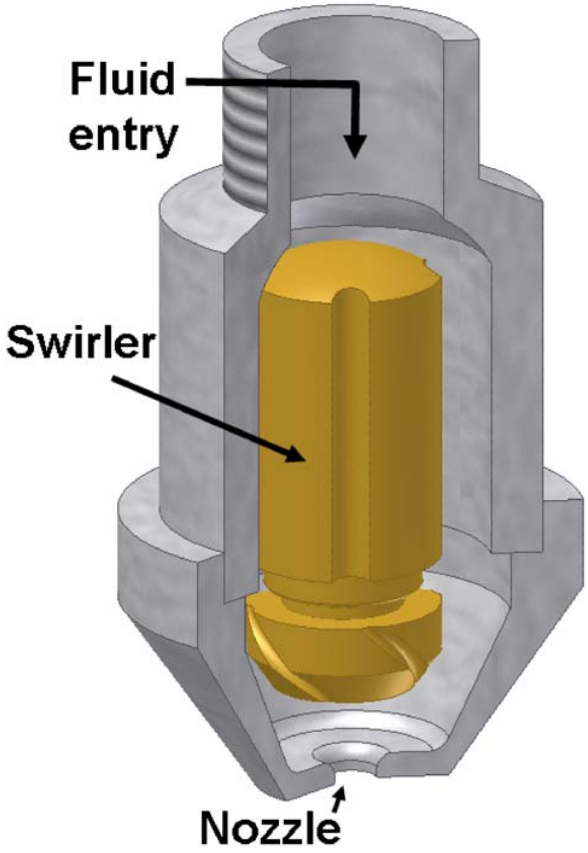

FIGURE 6. (Colour online) Cutaway view of the nozzle used for the production of oil sprays. The nozzle has a 45 degrees conical inlet. Diagram is to scale.

(0.1 kPa) at a frequency of 333 Hz. The modulation pressure amplitude used in the experiments presented in this paper (1%) corresponds to the minimum modulation required to cause stable break-up of the jet. Under this conditions, the jet breaks up at a distance of 27.5 cm from the nozzle plane (commonly called the break-up length).

The optical system used to visualize the centimeter-scale jets utilizes a vibration reduction Nikkor 18-55 mm f/3.5-5.6 lens mounted on a Nikon D80 DSLR camera body. This arrangement is set to produce a field of view of 34×23 cm, with a working distance of 45 cm and a depth of field of 5 cm. To obtain the shadowgraph illumination, single flashes were produced by phase-lock triggering of a SB-800 Speedlight Nikon Flash in the 1/128 option. This setting produces light pulses of $\approx$2 ms duration that are short enough to freeze the motion of the jet in the image. The flash was placed 2 m away from the jet and a generic projector screen was used as an optical diffuser, at a distance of 30 cm from the jet, to produce an even background illumination. The camera shutter was opened for 2 seconds in darkness so that the camera sensor only captured light from the flash. The triggering circuitry was locked to the phase of the sinusoidal modulation used to break up the jet. No illumination lens was used in this setup as the raw intensity of the flash perceived by the camera sensor at a sensitivity of 600 ISO was enough to produce high quality images with good contrast, as shown in Fig. 4. The uniformity of the background was adjusted by varying the relative position of the diffuser, the flash and the jet. The exposure time in this and the other two shadowgraph systems was controlled by the flash duration and not by the camera shutter, and only single-flash photography was used.

2.2. Sprays

The second shadowgraph system discussed here was developed for the study of sprays. Sprays and aerosols are used as dispensing systems in a wide range of applications, from the delivery of materials from pressurized canisters (*e.g.* paints, deodorants, insecticides, etc.) to the delivery of combustibles for burning (*e.g.* internal combustion engines and oil combustion for power generation). Typically, a spray or an aerosol

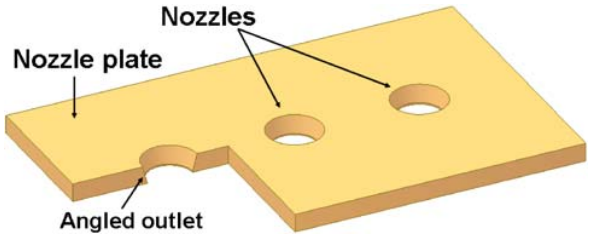

FIGURE 7. (Colour online) Schematic and cutaway view of part of the nozzle plate from a commercial ink-jet printhead (Xaar XJ126). The nozzle profile presents a conical inlet with a final diameter of ca. 50 μm. Relative sizes are in proportion.

is produced by the continuous flow of over-pressurized liquid through a nozzle. In a spray, the fluid emerges as a continuous jet until surface tension forces stretch and eventually break up the liquid into droplets, Fig. 5. The distribution of the droplets along the spray is determined by the fluid properties and also by aerodynamic effects. The analysis of shadowgraph images from sprays can be used to quantitatively obtain the droplet size distribution at different locations along the spray. This analysis can be used in practical applications to determine the optimum position of a substrate for spray deposition or the best position of an ignition element in a combustion chamber.

Sprays were formed by forcing oil through a generic swirler nozzle with an oil pump at a measured pressure of 460 kPa and a flow rate of 0.45 l/min; the geometry of the nozzle is shown in Fig. 6. After ejection, the fluid is collected and pumped back so that the process can be run continuously. The nozzle outlet diameter is 1.2 mm. Under these conditions the break-up process for quenching oil at 38°C starts to occur at approximately 1.2 cm from the nozzle plane, and spray droplets are first obtained at a distance of approximately 2.0 cm, as shown in Fig. 5.

The optical system used to visualize these sprays consists of an Apo Nikkor 305 F/9 lens attached to a 610 mm extension tube and mounted on a Nikon D80 DSLR camera body to produce a field of view of 23×31 mm, a working distance of 40 cm and a depth of field of approximately 17 mm. A single generic biconvex lens of 110 mm diameter and 320 mm focal length was used in the illumination system. This lens focused the light pulses produced by an argon jet stabilized spark generator (Pulse, Instrumentation and Controllers Ltd) on to a glass diffuser to produce the uniform background illumination. The nominal light pulse duration for this generator is 300 ns with an energy of 2.5 J. The spray generator was positioned 610 mm away from the camera lens and at 732 mm from the spark generator, resulting in uniform illumination. The triggering time of the spark generator was externally controlled by a series of SN74121 integrated circuits interconnected to produce time delays within the range of 5 to 150 ms. The camera sensor was set at a sensitivity of 400 ISO. As in the previous setup, the camera shutter was opened for 2 seconds in darkness and the exposure time controlled by the the spark duration. Examples of shadowgraph images of these sprays are shown in Fig. 5.

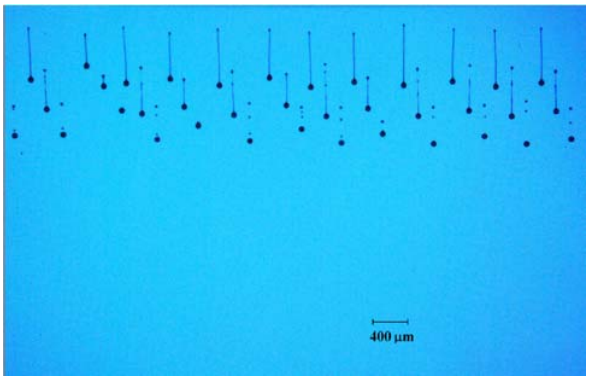

FIGURE 8. Figure caption.(Colour online) Shadowgraph picture of droplets jetted from a Xaar XJ126 printhead. The droplets travel at an speed of 5 m/s and have a volume of 80 picoliters.

2.3. Droplets

The third shadowgraph system was designed to visualize micrometer-size droplets from a commercially available ink-jet printhead. The aim of this study was to develop a technique to quantify the directionality (straightness) of individual droplets jetted from an ink-jet nozzle. The method uses double flash shadowgraph images of detached droplets generated by a row of nozzles to calculate the flight direction. This study is of interest to the ink-jet industry as it can be used to quantify the effect of defects on the behavior and reliability of printing nozzles or alternatively, to characterize the natural angular variability within an array of nozzles. The technique was tested with a commercially available printhead.

The droplets were produced with a Xaar XJ126 drop-on-demand (DoD) printhead which contains a linear array of 50 μm diameter nozzles, [4]. The fluid is ejected by the distortion of piezoelectric elements located between the ink chambers behind the nozzle plate. Typically, this printhead operates at droplet speeds of 5-6 m/s with droplet volumes of 80 picoliters. The nozzle has a conical inlet with a 30 degree included angle and has a depth of approximately 20 μm as shown in Fig. 7. The fluid used in these experiments is a transparent oil with a Newtonian viscosity of 20 mPa·s [4]. The optical system used to visualize the 50 μm droplets consists of a 12X zoom Navitar microscope lens with a 2x lens attachment mounted on a Nikon D40x DSLR camera body. This arrangement provides a working distance of 32 mm, a field of view of 3.5×2.4 mm and a depth of field of 500 μm. Under these conditions, the resolution of the image is 2.3 μm/pixel.

The system used to back-illuminate the droplets consisted of a dual-spark flash generator (High-Speed Photo-Systeme), a multimode fiber optic, a condenser lens, an array of two plano-convex lenses, an optical diffuser, a microscope lens and the camera sensor, as illustrated in Fig. 2. Each of the two spark flash generators, which can be independently triggered, produces flashes of 20 ns of duration with 25 mJ of

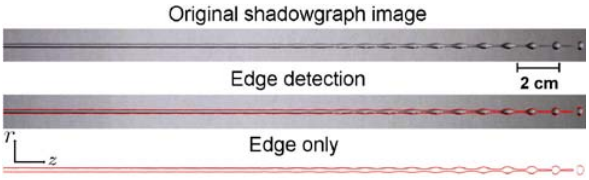

FIGURE 9. (Colour online) Steps in image processing. Raw image (above), processed image with edge detected (middle) and jet edge only (below).

energy. The light from both spark sources is focused by a condenser lens on to the end of the optical fiber. The light at the output of the fiber encountered an engineered optical diffuser (Thorlabs and RPC Photonics) and was then focused by the pair of plano-convex lenses. The first lens, with a 60 mm focal length, was positioned 35 mm from the diffuser. The second lens, with a 45 mm focal length, was placed 10 mm in front of the first lens and 150 mm from the front of the microscope lens. The droplets were generated in front of the array of lenses and at 35 mm from the microscope lens. A pulse generator (TTi) was used to trigger the spark flashes individually, separated by a time delay. The camera sensor was set at 600 ISO. An example of a single flash shadowgraph of an array of 38 droplets is shown in Fig. 8.

3. Image Analysis

The process of image analysis is based on the detection of fluid boundaries in shadowgraph pictures. As discussed above, the identification of features in images is nowadays a common function in image processing programs; among many examples, Matlab has a built-in routine called "bwtraceboundary" to outline object boundaries in black and white images, Labview has the "Threshold" tool on the NI Vision Assistant and HarFA and PEJET have a thresholding process for colour images, [13,14,4] and [15]. In this work, both HarFA and PEJET were used to analyze colour RGB shadowgraph images. Briefly, one way to identify the boundaries of the fluid regions is to compare the intensity levels of the RGB channels to a pre-established threshold level; this is actually the method used by HarFA, Matlab and Labview. Another way to detect the boundary, used by PEJET, is by identifying local changes of RGB intensity, which are at their largest at the fluid boundaries. This approach produces better results when the image background brightness is not perfectly even, [4]. In any case, the result of both approaches is highly dependent of the evenness of the background and the sharpness of the boundary, and as a consequence the correct design of the shadowgraph imaging setup is essential.

Once the fluid boundaries are detected and their coordinates recorded, several studies can be carried out. In this work, the boundary profiles obtained from the different systems were analyzed in different ways depending on the application.

3.1. Analysis of Jets

As noted above, continuous ink-jet (CIJ) printheads produce streams of droplets by harmonically disturbing a liquid (ink) jet. Most commercial CIJ printers recirculate and reuse the fluid that has been jetted but not used for printing. As this process is repeated, the concentration of the solvent or the ink components may change as a result of various factors such as evaporation, sedimentation and/or temperature variations. These processes modify the fluid properties, the jet break-up behavior and ultimately the behavior and spacing of the droplets, which can lead to reductions in print quality, [9]. Modern commercial printers have built-in rheometers and sensors that constantly monitor the viscosity and temperature of the ink, but other properties such as the surface tension remain unmeasured. This section reports a method where fluid properties (*e.g.* the surface tension) can be continuously monitored through the analysis of shadowgraph images of jets. This approach does not affect the jetting or the break-up process, and although it was tested on centimeter-long jets generated by a large nozzle, could readily be adapted to a nozzle at typical commercial CIJ scale (ca. 100 micrometer diameter).

The experimental setup described in Sec. 2A was used to jet a viscous Newtonian liquid consisting of a solution of 74.7% glycerol (99.9% pure) in water with the following measured properties: density ρ =1250 kg/m^3, surface tension σ = 81.0 $\pm$ 0.5 mN/m and viscosity μ = 36.7 $\pm$ 0.2 mPa·s. Surface tension and viscosity of the fluid were measured using a bubble pressure tensiometer (SITA Messtechnik, Pro line t15, at a bubble lifetime of 100 ms) and a portable viscometer (Hidramotion, Viscolite 700). The liquid was jetted through a 2.2 ± 0.05 mm diameter nozzle and the driving pressure was modulated with a sinusoidal waveform with an amplitude of 100 Pa. The resulting jet was imaged as described above and the images were analyzed as follows. First, the image was cropped from its original size (3872$\times$2592 pixels) to a smaller format (3144$\times$151 pixels) to show only the field of view corresponding to the modulated jet and the first few separate droplets (the resolution of the image was of 114$\pm$1 pixels/cm). This step is necessary to speed up the analysis and avoid the contour detection of features extraneous to the jet. Next, the image was analyzed, the jet profile detected and its contour recorded. This process is illustrated in Fig. 9. Both the shadowgraph image and the surface profile can be studied to quantitatively determine jet properties. The jet axial speed (v) can be obtained directly by measuring the droplet separation using a relationship obtained from mass and flow conservation:

$$v = f\lambda \tag{1}$$

where λ is the wavelength of the surface disturbance or the droplet separation after break-up and f is the imposed modulation frequency [9]. The droplet separation (wavelength) can be accurately measured by calculating the center of mass of the droplets from the contour analysis or via a spatial fast Fourier transform (FFT) of the radial jet profile. These methods produce a value of $\lambda = 10.5 \pm 0.2$ mm. In addition to

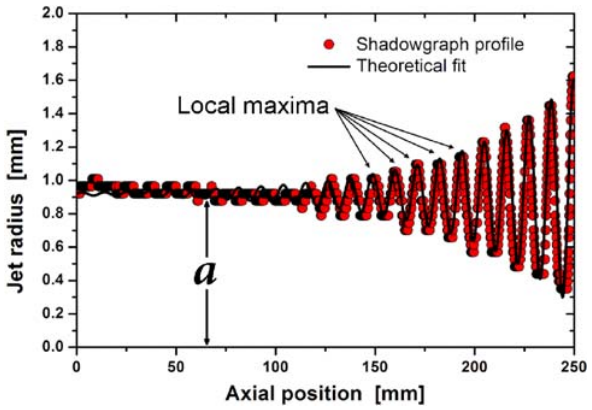

FIGURE 10. (Colour online) Experimental and theoretical instantaneous jet profiles in terms of the axial position of a modulated viscous jet. The experimental profile was obtain by analysis of shadowgraph images.

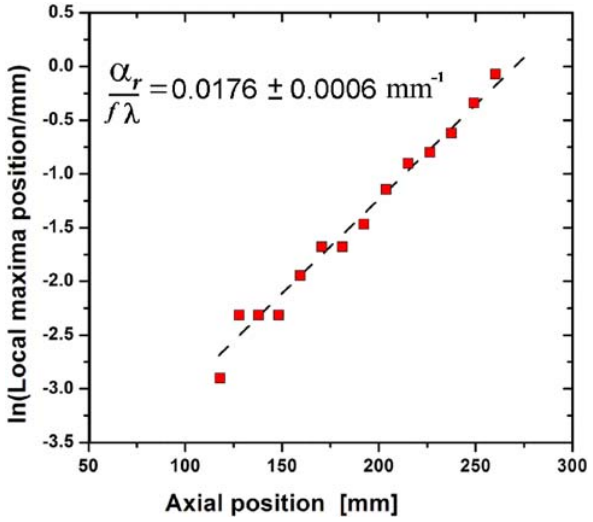

FIGURE 11. (Colour online) Logarithm of the position of the instantaneous jet surface local maxima (from the initial radius) from an instantaneous shadowgraph image of a continuous modulated jet. The slope of the data corresponds to the growth rate of the jet disturbance.

this simple analysis, the growth of the disturbance observed on the jet profile can provide information about the fluid dynamic properties. Rayleigh and Weber derived expressions that describe the exponential grow of surface perturbations in harmonically disturbed cylindrical jets [2]. In cylindrical coordinates, the surface profile of a weakly harmonically-disturbed jet is given by

$$r = a + \xi_0 \mathrm{e}^{ikz+(\alpha_r+i2\pi f)z/v}, \tag{2}$$

where a constant axial speed (v) is assumed, a is the initial radius, and ξ_0, k, and α_r are the initial amplitude, the wave number and the growth rate of the disturbance respectively; $k = 2\pi/\lambda$. The growth rate depends on the fluid properties and for Newtonian viscous fluids is given by

$$\alpha_r^2 \frac{kaI_0(ka)}{2I_1(ka)} + \alpha_r k^2 \frac{\mu}{\rho}\left[2ka\frac{I_0(ka)}{I_1(ka)}\frac{l^2}{l^2-k^2} - 1 - 2la\frac{I_0(la)}{I_1(la)}\frac{k^2}{l^2-k^2}\right] = \frac{\sigma k^2}{2\rho a}(1-k^2a^2), \tag{3}$$

where $l = k^2 + \rho/\mu$. A detailed derivation of these expressions can be found in Ref. 2. It is through Eq. 3 and the profile obtained by the image analysis that jet properties can be determined as shown in Fig. 10. The initial radius (a) is calculated by averaging the section of the radial profile corresponding to the first few surface oscillations (the first 5 oscillations were used in this example although this number is not critical as the disturbance is only detectable after about 10 oscillations). The growth rate (α_r) is obtained from a linear regression analysis, as the slope of the logarithmic position of the local maxima of the surface disturbance (Figs. 10 and 11). As the value of the growth rate is theoretically determined by Eq. (3) and the fluid properties, this analysis can be utilized to study the variation of the fluid properties over time.

To test this method, shadowgraph images of a modulated jet were analyzed and the jet profile compared with the profile predicted from Rayleigh's model. The theoretical expression for the jet profile with the measured fluid properties produces a growth rate value of $\alpha_r = 60.2 \pm 2.0$ s^{-1}. In contrast, from the slope value shown in Fig. 11, the image analysis gives a value of $\alpha_r = 61.5 \pm 3.3$ s^{-1}, which is consistent with the prediction within experimental errors. The shadowgraph jet profile is shown in Fig. 10 together with the theoretical curve predicted from the measured fluid properties, the nozzle diameter and an initial disturbance amplitude calculated by recursive fitting; the close agreement is evident. This analysis is of interest to the inkjet community as is can be used to monitor fluid properties that tend to vary during the operation of their printhead systems [16].

3.2. Analysis of sprays

The delivery of liquid through sprays and aerosols is a technique widely used in manufacturing and other industrial processes. The atomization process occurs as a result of the interaction between the liquid and the surrounding air, and involves several stages through which the oil eventually becomes an aerosol. Figure 12 shows a transparent oil spray produced by the pressure atomizer described above. Spray generation is similar to other types of jetting such as CIJ or DoD ink-jet printing as the liquid passes generally through three stages. In the first, the liquid is discharged as a jet; this step is easily recognized as the jetted liquid can still be identified as a single continuous region (*i*). In the second stage, the liquid is extended and stretched to form liquid threads or ligaments (*ii*). The last stage is identified by the collapse or break-up of these ligaments into droplets by surface tension

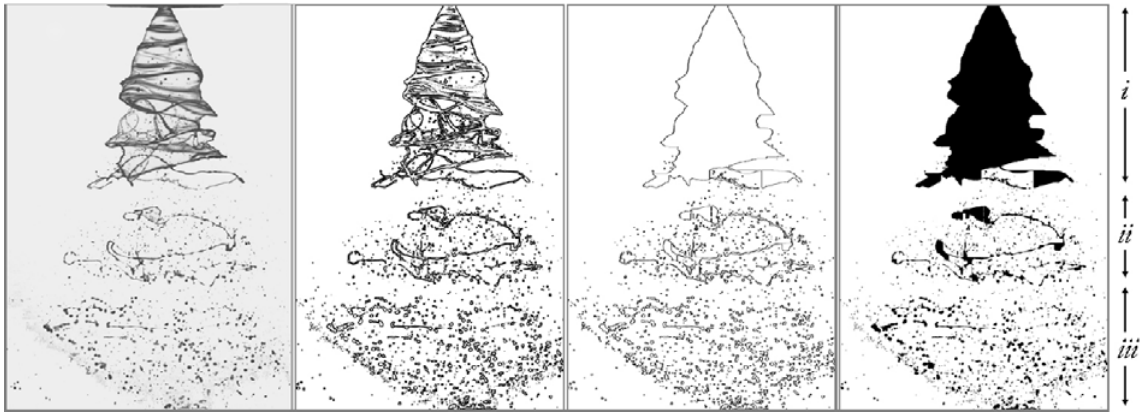

FIGURE 12. (Colour online) Steps in image processing applied to a shadowgraph image of an oil spray. Raw image (far left), processed image after contour detection, (middle-left), liquid boundary (middle right) and individual features (far right). Three characteristic stages are observed as indicated: i single-body jet, ii ligament regime and iii droplet domain.

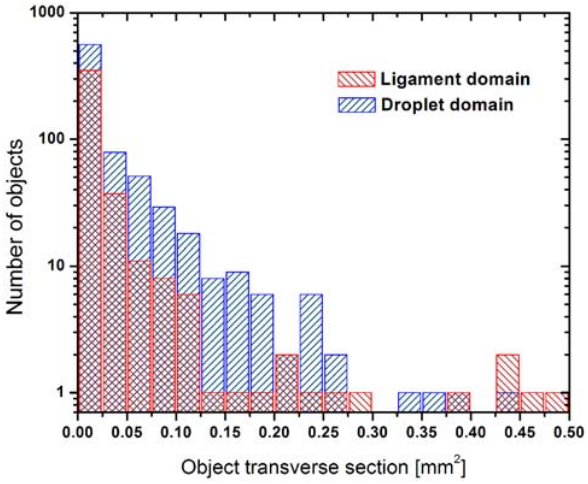

FIGURE 13. (Colour online). Liquid feature size distribution in the ligament (in red) and droplet (in blue) domains of a liquid spray. Please note the logarithmic scale on the vertical axis.

forces (*iii*). Downstream, these droplets can achieve, under some conditions, a terminal homogeneous velocity of several meters per second. In a similar way to the CIJ case, the jetting process of sprays depends on several variables such as the nozzle geometry, the liquid properties and the driving pressure. These properties govern the droplet size and speed distributions and may change in time depending on the conditions under which the dispensing system is operated. Unlike CIJ, sprays are not forced or modulated to break up at a well-determined frequency to produce droplets periodically. As a consequence the break-up of liquid sprays is random and so are the droplet separation and volume making their characterization difficult. This section describes an imagining method to monitor the size distribution of droplets generated by a spray dispenser. The method is non intrusive and does not affect the operation or the spray mechanisms.

The experimental setup described in Sec. 2B was utilized to discharge quenching oil through a 1.2 mm diameter nozzle into air. The image analysis of the captured sprays consists of the study and identification of the fluid edges within a selected area of interest. This process requires the detailed examination of these boundaries to determine which side of the edges correspond to the liquid and which side does not; a similar method is described for droplets in Ref. 4. This is necessary when shadowgraph images of transparent liquids are analyzed as some of the flash light can be refracted through the liquid onto the camera sensor and not away from it. This effect is visible in the left-hand image in Fig. 12 where the liquid in the upper part of the spray is transmitting light from the background and the internal structure of the liquid is visible. This internal structure needs to be excluded from the image analysis as it can be wrongly recognized as part of the fluid boundary; as seen on the middle-left image of Fig. 12. With the fluid boundaries detected, an algorithm that identifies the outermost closed boundary is used to filter out all the unwanted features, [4]. The results of this process are seen in the third image of Fig. 12.

Once the real features are detected and labeled, their pixels positions are recorded. To estimate the size of individual liquid features, the transverse section (or the projected area) of the objects is calculated as the number of pixels contained inside their boundary. This process is illustrated on the far-right image on Fig. 12 where fluid edges have been filled to reconstruct the transverse section of features. Although the precise volume of the features recorded in regions *i* and *ii* (given the lack of cylindrical or spherical symmetry) cannot be calculated with this technique, the measured transverse sections can be utilized to estimate the feature size distribution along the spray. The histogram in Fig. 13 shows the number of features or objects in terms of their projected area within a spray section. Figure 13 indicates that the predominant size in both domains corresponds to a feature size of around 0.03 mm^2. The histogram also shows that there are

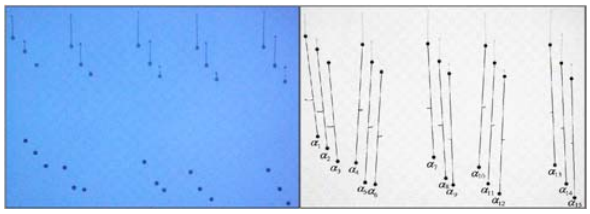

FIGURE 14. (Colour online) Raw image (left) and processed version (right) of a double-flash shadowgraph picture of a set of 15 droplets. The droplets on the top are recorded during the first flash event and the ones at the bottom during the second fash. The droplet deviation angle is determined from the position of the droplet at the first flash and its position after 480 μs.

twice as many objects of this size in the droplet domain as in the filament domain, showing that filaments are broken up into droplets of that size.

Although this technique is not adequate to measure the volumetric distribution, it can be used in industrial applications to monitor the break-up behavior of sprays by monitoring changes on the size distribution. However, in the droplet domain, as most features have a circular cross section, the results of the image analysis could also be used to estimate the volume distribution by simple geometry as described in Ref. 4.

3.3. Analysis of droplets

Droplets provide an excellent method to deposit liquid materials. One of the most successful examples of their practical use in industry is in ink-jet printing. As in jets and sprays, the behavior of printed droplets is governed by the liquid properties, the jet driving pressure and the dimensions of the nozzle, and is affected by other factors such as nozzle imperfections, the presence of dried ink around the nozzle, inhomogeneities in the piezoelectric driving elements and in the nozzle plate material, and the presence of gas bubbles in the printhead chambers, [9] and [17]. Jet directionality is a key parameter as it influences the quality of printing. Although jet directionality is a key parameter as it influences the quality of printing, the effect on jet directionality of nozzle properties is a topic which has not been extensively studied because most theoretical models and numerical simulations assume symmetrical geometries or are valid only for specific liquid properties (*i.e.* Newtonian liquids, [18,19] and [20]). This section describes a method for characterizing the directionality of jets by shadowgraph imagining of droplets.

Jets and droplets were produced from a Xaar XJ126 printhead and recorded with the shadowgraph system described in Sec. 2. Briefly, the image analysis calculates the jetting angle by detecting the droplet positions at two times defined by two flash events; this analysis is shown schematically in Fig. 14. First, an image is analyzed to detect the edges of the liquid droplets. Next, the positions of the droplet boundaries are used to calculate its center of mass (the center of mass position being determined using the method described in

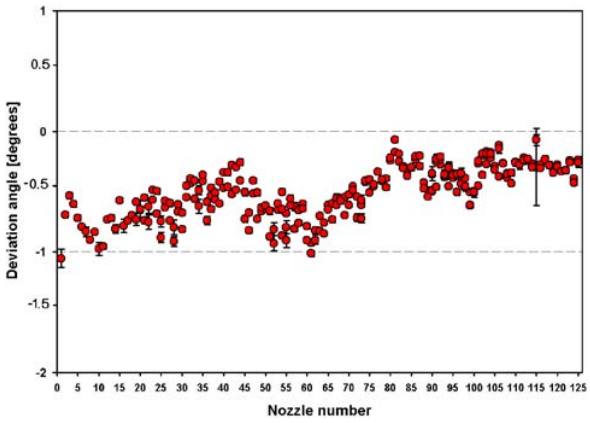

FIGURE 15. (Colour online) Results from the image analysis of double-flash shadowgraph images. The error bars are the result of 5 consecutive experiments.

Ref. 4. Finally, the positions of the centers of masses are corrected for lens distortion and the angle formed between the droplet position at the two flashes events is then calculated and recorded. During the analysis, the original image is divided into sections where each portion contains only the images of one single droplet recorded by the two flashes. For these experiments, the field of view of the imaging system permitted the visualization of 36 or 37 jets in a single image, as shown in Fig. 8. During the analysis, these images were divided into slices with widths equal to the nozzle pitch of the printhead (140 μm). Pincushion distortion is removed by a third-order polynomial correction algorithm whose coefficients were obtained through the imaging and correction of an accurate square mesh object pattern from a microscope grating. This analysis was applied to images corresponding to all 126 nozzles of the Xaar printhead; some of the results are shown in Fig. 15. As a result, these experiments confirmed the reported native jet variability stated by the printhead manufacturer (reported to be $<$1 degree).

This non-intrusive imaging technique could be used in industrial applications to assess the jetting directionality of individual nozzles in a printhead.

4. Conclusions

Image analysis methods have been developed and applied to shadowgraph images obtained from three different experimental setups to study three industrial methods for the delivery of liquids: continuous inkjets, continuous sprays, and droplets jetted from a drop-on-demand inkjet printhead. These methods produce quantitative data that can be used to monitor processes such as printing and spraying.

It has been shown that shadowgraph imaging can be utilized to monitor variations on the liquid properties of continuous modulated jets by the analysis of their profile. In the case of sprays, these experiments have shown that the analysis of shadowgraph images can be used to estimate the drop size distribution and its variation with distance from the noz-

zle. This method could be used to monitor and/or control the behavior of a spray in order to deliver a certain distribution of droplet size at some distance from the nozzle. In the field of inkjet printing, these experiments were used to asses the nozzle directionality and could be used on a production line to test the properties of fabricated printheads.

All these imaging techniques are non-intrusive and can be applied continuously during the jetting process.

Acknowledgments

This work was supported by the Engineering and Physical Sciences Research Council (UK) and industrial partners in the Next Generation Ink-jet Printing project.

1. G.S. Settles, *Schlieren and Shadowgraph Techniques: Visualizing Phenomena in Transparent Media* (Springer, Heidelberg 2001).
2. G. Brenn, Z. Liu, and F. Durst, *International Journal of Multiphase Flow* **26** (2000) 1621.
3. L. Le Moyne, V. Freire, and D.Q. Conde, *Chaos, Solitons and Fractals* **38** (2008) 696.
4. I.M. Hutchings, G.D. Martin, and S.D. Hoath, *Journal of Imaging Science and Technology* **51** (2007) 438.
5. A. Frohn and N. Roth, *Dynamics of Droplets* (Springer Verlag, Berlin 2000).
6. D. González-Mendizabal, C. Olivera-Fuentes, and J.M. Guzmán, *Chem. Eng. Comm* **56** (1987) 117.
7. M. Levanoni, *IBM. J. Res. Develop* **21** (1977) 56.
8. S.A. Curry and H. Portig, *IBM. J. Res. Develop* **21** (1977) 10.
9. C.A. Bruce, *IBM. J. Res. Develop* **20** (1976) 258.
10. J.R. Castrejón-Pita, G. Martin, S. Hoath and I. Hutchings, *Rev. Sci. Instrm.* **79** (2008) 075108.
11. L. Rayleigh, *Proc. Lond. Math. Soc.* **10** (1878) 71.
12. C. Weber, *Z. Angew Math. Mech* **11** (1931) 136.
13. M. Nezadal and O. Zmeskal, *Harmonic and Fractal Image Analyzer* (code) (2001), e-Archive: http://www.fch.vutbr.cz/lectures/imagesci
14. K. Tomankova, P. Jerabkova, O. Zmeskal, M. Vesela, and J. Haderka, *Journal of Imaging Science and Technology*, **50** 583 (2006).
15. J.C. Russ, *The imaging Processing Handbook* 4th ed. (CRC Press, Boca Raton, 2002).
16. V.P. Janule, *Pigment and Resin Technology* **25** (1996) 10.
17. J. de Jong *et al.*, *J. Acoust. Soc. Am.* **120** (2006) 1257.
18. N.F. Morrison and O.G. Harlen, *Rheol. Acta* DOI: 10.1007/s00397-009-0419-z (2010).
19. C.S. Kim *et al.*, *Computers & Fluids* **38** (2009) 602.
20. A.S. Yang, C.H. Cheng and C.T. Lin, *J. Mechanical Engineering Science: Proc. IMechE 2006* **220** (2006) 435.